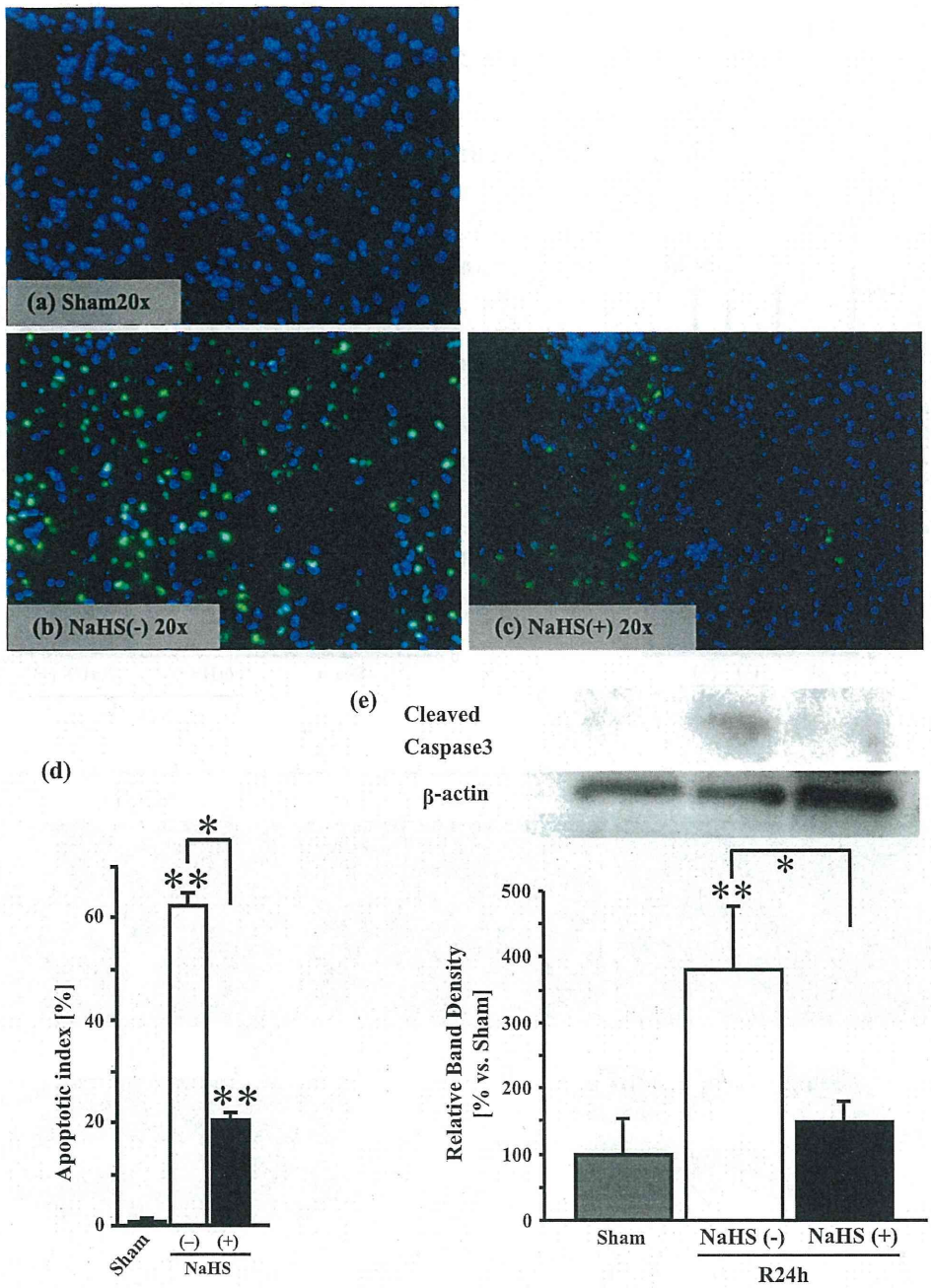

Fig. 4 Sodium hydrogen sulfide (NaHS) attenuates apoptosis of hepatocytes. Mice were subjected to partial warm ischemia for 75 min and subsequent reperfusion (I/R) for 24 h. Liver sections were stained by the fluorescent TUNEL method and nuclear counterstaining with DAPI. Representative photographs (20× magnification) are shown. **a** Sham operation. **b** NaHS (−): I/R with vehicle treatment. **c** NaHS (+): I/R with NaHS (1.0 mg/kg) administration before reperfusion. **d** The apoptotic index was calculated as the number of TUNEL-positive cells divided by the number of DAPI-positive cells. Data are expressed as the mean ± SD. **e** Cytosolic protein of the ischemic lobe at R6 h was applied to a standard western blot. Representative western blots detected by cleaved caspase-3 antibody (*top*) and the ratio of the relative intensity, cleaved caspase-3/β-actin (*bottom*), are shown. Each normalized value was further normalized by the mean value in the sham group, and expressed as the mean ± SD. $^{*}P < 0.05$, NaHS (−) vs. NaHS (+). $^{**}P < 0.05$ vs. Sham

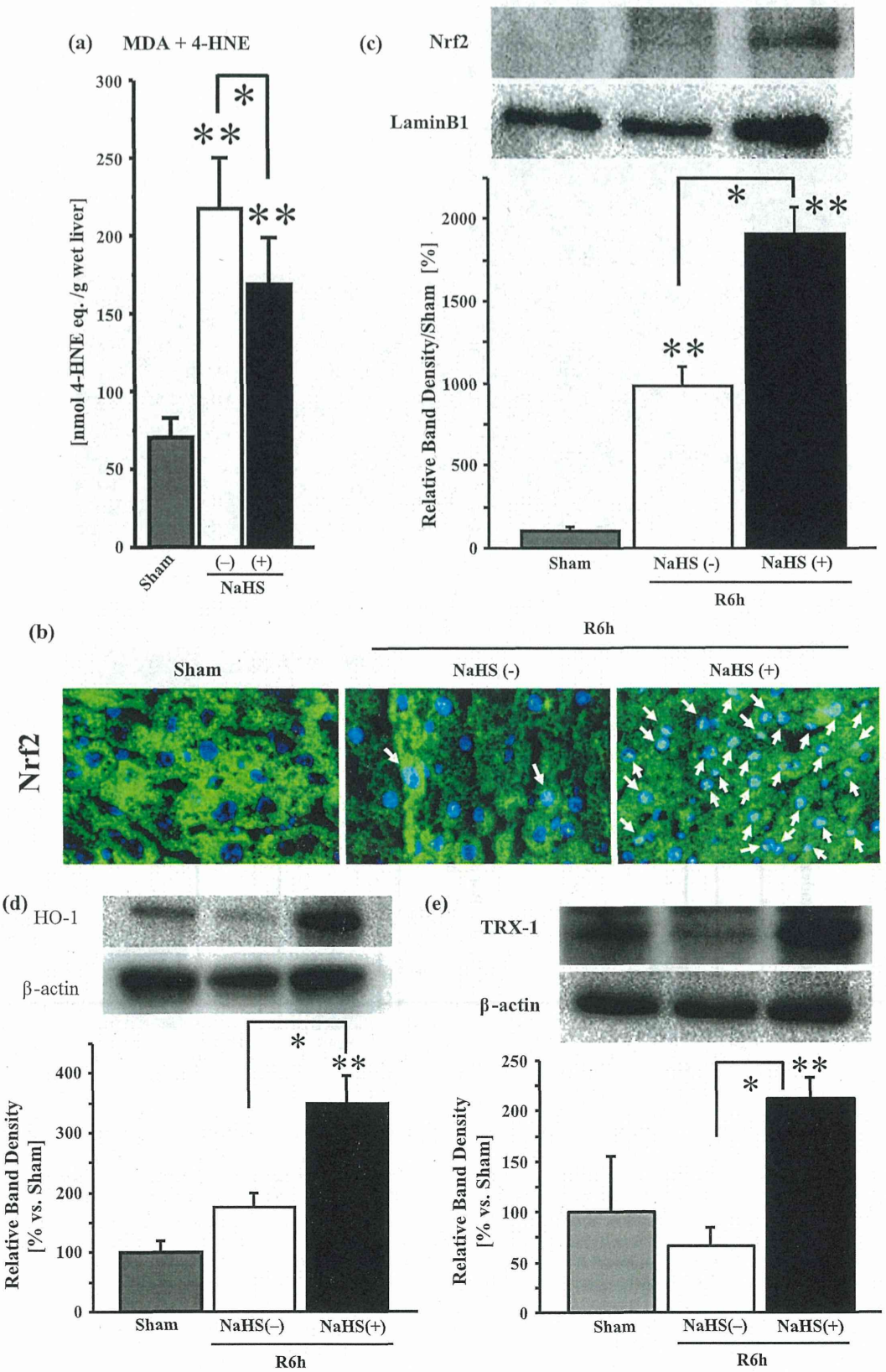
(a) MDA + 4-HNE
[nmol 4-HNE eq. /g wet liver]
300
250
200
150
100
50
0
Sham
(–) (+)
NaHS
(c) Nrf2
LaminB1
Relative Band Density/Sham [%]
2000
1500
1000
500
0
Sham
NaHS (-)
NaHS (+)
R6h
(b)
R6h
Sham
NaHS (-)
NaHS (+)
Nrf2
(d) HO-1
β-actin
Relative Band Density [% vs. Sham]
400
300
200
100
0
Sham
NaHS(–)
NaHS(+)
R6h
(e)
TRX-1
β-actin
Relative Band Density [% vs. Sham]
250
200
150
100
50
0
Sham
NaHS(–)
NaHS(+)
R6h

◀ **Fig. 5** Sodium hydrogen sulfide (NaHS) reduces oxidative stress. Mice were subjected to partial warm ischemia for 75 min and subsequent reperfusion (I/R) for 6 h. **a** Lipid peroxidation was assessed by MDA + 4-HNE. **b** Representative photographs (40× magnification) are shown. Immunohistochemistry of the liver showed that Nrf2 (*Green*) was ubiquitous in the cytosol but not in the nucleus in the sham-operated group. In the NaHS (−) group, only faint staining of Nrf2 in the nucleus was seen, whereas in the NaHS (+) group, almost all cells showed Nrf2-positive (*pale blue*; *Arrow*). **c** Western blot of nuclear proteins with regard to Nrf2. **d** Western blots of cytosolic proteins were evaluated for the HO-1 protein, and **e** thioredoxin-1 (TRX-1). Representative western blots (*top*) and the relative ratio (target protein/β-actin) (*bottom*) are shown. Each normalized value was further normalized by the mean value in the sham-operated group. Data are expressed as the mean ± SD. $*P < 0.05$, NaHS (−) vs. NaHS (+). $**P < 0.05$ vs. Sham

significantly higher in the NaHS treatment group than in the other groups (Fig. 3c, d).

Apoptosis

TUNEL staining at R24 h showed almost no positive cells in the sham group (Fig. 4a, d). TUNEL-positive cells were augmented by hepatic warm I/R in the NaHS(−) group at R24 h (Fig. 4b, d), whereas they were significantly reduced by NaHS treatment (Fig. 4c, d). Cleaved caspase-3 at R6 h was significantly augmented by hepatic warm I/R in the NaHS(−) group, whereas it was significantly suppressed by NaHS treatment (Fig. 4e).

Oxidative stress

We calculated the sum of the values of malondialdehyde (MDA) and 4-hydroxy-2-nonenal (4-HNE), the end products of lipid peroxidation, at R6 h. This value was augmented by hepatic warm I/R in the NaHS(−) group, whereas it was significantly reduced by NaHS treatment (Fig. 5a).

Anti-oxidative responses were evaluated by the translocation of Nrf2 and expression of the downstream enzymes, HO-1 and TRX-1. Immunohistochemistry of Nrf2 (Green) reveled homogeneous staining in the cytosol, but not in the nucleus, in the sham-operated group. In the NaHS (−) group, there was only faint staining of Nrf2 in the nucleus, whereas in the NaHS (+) group, almost all cells showed Nrf2-positive nucleus (pale blue; arrow), indicating that NaHS treatment augmented the nuclear translocation of Nrf2 at R6 h (Fig. 5b).

The western blot of nuclear proteins revealed that the sham group had the lowest value. The value in the NaHS(−) group at R6 h was increased significantly, and it was further increased significantly in the NaHS(+) group (Fig. 5c). The expression of HO-1 in the cytosol was increased by hepatic warm I/R in the NaHS(−) group, and it was further augmented significantly by NaHS treatment (Fig. 5d). The expression of TRX-1 in the cytosol showed a tendency to decrease with hepatic warm I/R in the NaHS(−) group, whereas it was significantly augmented by NaHS treatment (Fig. 5e).

Proliferation

Hepatic proliferation was evaluated by PCNA staining at R24 h (Fig. 6a–d). In the sham group, the percentage of PCNA-positive hepatocytes was 47 ± 14 %. The positive rate was reduced significantly to 13 ± 15 % in the NaHS(−) group, whereas it was augmented significantly to 63 ± 14 % by NaHS treatment.

Discussion

We confirmed the beneficial effects of NaHS against warm I/R of the mouse liver, by demonstrating a reduction in tissue injury, apoptosis, oxidative damage, and inflammatory reactions, with stimulation of liver regeneration. These beneficial effects were at least in part due to the augmented nuclear translocation of Nrf2 and downstream activation of anti-inflammatory and anti-oxidant pathways. Activation of the pro-survival signals was demonstrated by the augmented phosphorylation of PDK-1, Akt, mTOR, and p70s6k in response to NaHS treatment. Simultaneous activation of anti-apoptotic, anti-inflammatory, anti-oxidative, pro-survival, and pro-proliferation cascades appeared to allow recovery of the liver subjected to warm I/R.

Hydrogen sulfide (H_2S) is produced endogenously from cysteine in the liver, kidney, vessels, brain, and nerves, and its exertion at low concentrations is biologically important [23]. Furthermore, H_2S has been reported to reduce IRI of the liver [13–16] and other organs [9–12]. Consistent with these reports, the present study showed a reduction in net injury by ALT leakage and histopathology.

Acute inflammation in hepatic IRI is initiated mainly in Kupffer cells and hepatocytes during warm ischemia [2, 3, 24]. These cells release TNF-α, IL-6, and IL-1β, and stimulate inflammation, which in turn activates the cell death pathway, and ROS and protease release from neutrophils [3, 4]. Schlegel et al. [25] reported that serum TNF-α, IL-17, and the ratio of CD154-positive T cells were increased in a DCD liver graft after transplantation. IL-23 and Th17 cells, including NK, NKT, and γδT cells, play major roles in both acquired and innate immunity in organ transplantation [26]. In hepatic IRI, IL-23 stimulates Kupffer cells and CD4 +/Th17 cells. IL-6 released from Kupffer cells promotes further activation of Th17 cells to release IL-17, and stimulates neutrophil accumulation [27]. A recent report revealed that activation of CD40-CD40L (CD154) promoted oxidative stress-induced apoptosis in hepatocytes [28].

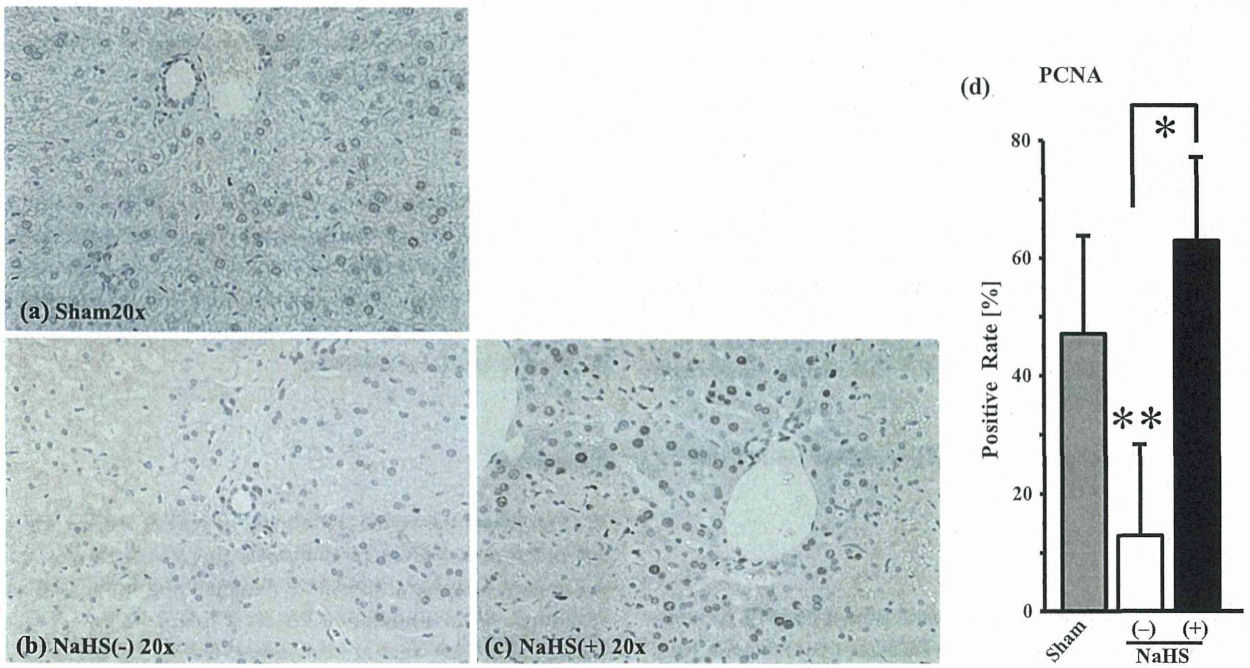

Fig. 6 Sodium hydrogen sulfide (NaHS) stimulates liver regeneration. Mice were subjected to partial warm ischemia for 75 min and subsequent reperfusion (I/R) for 24 h. Liver sections were stained by the anti-proliferating cell nuclear antigen (PCNA) antibody and hematoxylin as nuclear counterstaining. Representative photographs (20× magnification) are shown. In the sham group (**a**), the positive rate was 47 %, but it was significantly decreased in the NaHS(−) group (**b**), and it was significantly augmented in the NaHS(+) group (**c**). The rate of PCNA-positive hepatocytes is shown in (**d**). Values are expressed as the mean ± SD. $*P < 0.05$, NaHS (−) vs. NaHS (+). $**P < 0.05$ vs. Sham

In this study, serum TNF-α, IL-6, IL-1β, IFN-γ, IL-17, IL-23, and soluble CD40L (CD154) increased significantly within 3 h of reperfusion, but these changes were inhibited by NaHS. Hydrogen sulfide reduced hepatic IRI with less production of TNFα and IL-6 [16]. Suppression of the IL23–IL17 axis reduced hepatic IRI [29]. Altogether, these facts suggest that NaHS reduced hepatic IRI by inhibiting the IL23–IL17 axis, thereby inhibiting the activation of Kupffer cells, neutrophils, and lymphocytes (CD4 +/Th17 cells) in the early phase of reperfusion. Although there are various sources of CD40L, the main source is the activated platelets [30], and CD40L was found to worsen hepatic IRI [28]. In this study, there was a massive release of cytokines and chemokines at R3 h. Multiple pro-inflammatory mediators from various cell types, platelet-endothelial adhesion, and platelet-leukocyte aggregation would stimulate the further activation of platelets [2], leading to the sustained high level of soluble CD40L.

Oxidative stress is another important factor in hepatic IRI [2–4]. Oxidative damage in the sinusoidal endothelial cells stimulates endothelin-1 (ET-1) production, leading to microcirculatory disturbance [31, 32]. Several distinct mechanisms of the anti-oxidant property of H_2S have been reported, namely, direct scavenging of ROS [33], reversible inhibition of mitochondrial respiration [34], augmentation of glutathione (GSH) production through enhanced cystine/cysteine transport [35], and Nrf2-dependent expression of anti-oxidant and anti-inflammatory proteins [23]. Consistent with these reports, NaHS reduced lipid peroxidation and inflammation in this study.

Nrf2 exists in the cytosol with Keap-1 in the resting state, but it dissociates from Keap-1 on exposure to stimuli, such as oxidative stress and pro-survival signals, leading to up-regulation of HO-1 [36] and TRX-1 [37]. HO-1 reduces oxidative stress through the conversion of heme into biliverdin and carbon monoxide (CO) [38]. Furthermore, CO exerts anti-inflammatory and vasodilatory effects [39] and TRX-1 reduces protein thiol and/or hydrogen peroxide with the support of GSH [40]. In line with these reports, our study showed, for what we believe to be the first time, that NaHS augmented HO-1 and TRX-1 levels through augmented nuclear translocation of Nrf2, leading to reductions in oxidative stress and inflammation.

The anti-apoptotic and pro-survival effects of H_2S against mitochondria would result in an inhibition of intrinsic apoptosis [36]. H_2S activates this pathway in the I/R of hippocampal neurons [7, 41] and myocardium [5]. Insulin supplementation has been shown to stimulate

myocardial surviving expression via activation of PI3K-Akt-mTOR-p70s6k, resulting in anti-apoptotic effects [42]. In this study, pro-survival signals mediated by the PDK-1-Akt-mTOR-p70s6k axis were maintained by the higher phosphorylation in the NaHS-treated liver. Phosphorylation of p70s6k confers protection against IRI in the heart and small intestines through anti-apoptotic and anti-inflammatory effects [17, 18]. The enhanced PDK1-Akt signal reduced IRI through the augmented phosphorylation of PDK1 [43] and Akt [14], but not through de novo gene expression of these proteins, at least within 6 h of reperfusion. In line with these reports, this study is the first to show that NaHS supplementation ameliorated hepatic warm IRI by maintaining the phosphorylation of p70s6k and upstream kinases, including mTOR, Akt, and PDK-1. Since we did not assess any gene expression, further study is required to clarify the precise mechanism of NaHS-mediated protection during the early phase of reperfusion.

Another important anti-apoptotic signal in hepatic IRI is the signal transducer and activator of transcription 3 (STAT3) [9]. Ke et al. [29] recently reported that HO-1 ameliorated hepatic inflammation, apoptosis, and net injury after warm I/R by inhibiting NF-kappaB signals in the nucleus. They showed that STAT3 was indispensable for the HO-1-mediated down-regulation of TLR-4 and PTEN, and the augmentation of phospho-Akt. In the present study we observed a transient rise of IL-6 at 3 h, only slight increases of IL-6 and TNF-α at 6 h, and a significantly higher PCNA-positivity rate 24 h after reperfusion in the NaHS-treated group. Debonera et al. [44] reported that IL-6-mediated activation of STAT3 did not trigger liver regeneration in severely injured liver grafts. Although we did not evaluate STAT3 here, these observations suggest that the STAT3-mediated machinery of liver regeneration [45] would have functioned well in the NaHS-treated liver.

Recently, Zhang et al. [46] reported that NaHS administration before ischemia inhibited mitochondrial permeability transition pore opening and activated Akt-GSK3β. Exogenously administered hydrogen sulfide disappeared rapidly from the blood and tissues through oxidation and thiol-binding [47], with half-lives of 2.0 and 5.4 min in the aerobic and anaerobic liver, respectively [48]. Therefore, we administered NaHS before reperfusion to maintain enough concentration at reperfusion. In contrast to the previous report [46], we failed to show the efficacy by administration before ischemia in our preliminary study. In relation to dosage, Kang et al. [15] reported the effective dose to be 0.78 mg/kg. Since 0.5 mg/kg was less effective than 1 mg/kg, and 3 mg/kg resulted in animal death by respiratory dysfunction in our preliminary study, we adopted 1 mg/kg as the optimal dose (data not shown). The controversy might be due to the differences in ischemia time, species, and strain. Although further investigation is necessary to establish the optimal mode of administration for liver graft protection, it is encouraging that hydrogen sulfide proved effective when administered before ischemia [46], before reperfusion, and during cold preservation [49].

In conclusion, NaHS treatment against hepatic warm I/R resulted in high phosphorylation levels of PDK1, Akt, mTOR, and p70S6k, and nuclear translocation of Nrf2, leading to anti-oxidant, anti-inflammatory, anti-apoptotic, pro-survival, and pro-proliferative effects, and eventually reduced net IRI with rapid liver regeneration.

Acknowledgments We thank Mr. Masatoshi Horigome and Ms. Sayaka Miyoshi for their excellent technical support. This work was supported in part by a Public Trust Surgery Fund (2012) and a grant-in aid for Scientific Research from the Ministry of Education, Science, Sports, and Culture of Japan (No. 25293272).

Conflict of interest Shingo Shimada and his co-authors have no conflicts of interest.

References

1. Monbaliu D, Pirenne J, Talbot D. Liver transplantation using donation after cardiac death donors. J Hepatol. 2012;56:474–85.
2. Vollmar B, Menger MD. The hepatic microcirculation: mechanistic contributions and therapeutic targets in liver injury and repair. Physiol Rev. 2009;89:1269–339.
3. Zwacka RM, Zhou W, Zhang Y, Darby CJ, Dudus L, Halldorson J, et al. Redox gene therapy for ischemia/reperfusion injury of the liver reduces AP1 and NF-kappaB activation. Nat Med. 1998;4:698–704.
4. Abu-Amara M, Yang SY, Tapuria N, Fuller B, Davidson B, Seifalian A. Liver ischemia/reperfusion injury: processes in inflammatory networks—a review. Liver Transpl. 2010;16:1016–32.
5. Hu Y, Chen X, Pan TT, Neo KL, Lee SW, Khin ES, et al. Cardioprotection induced by hydrogen sulfide preconditioning involves activation of ERK and PI3 K/Akt pathways. Pflugers Arch. 2008;455:607–16.
6. Tsang A, Hausenloy DJ, Mocanu MM, Yellon DM. Postconditioning: a form of "modified reperfusion" protects the myocardium by activating the phosphatidylinositol 3-kinase-Akt pathway. Circ Res. 2004;95:230–2.
7. Noshita N, Lewen A, Sugawara T, Chan PH. Evidence of phosphorylation of Akt and neuronal survival after transient focal cerebral ischemia in mice. J Cereb Blood Flow Metab. 2001;21:1442–50.
8. King AL, Lefer DJ. Cytoprotective actions of hydrogen sulfide in ischaemia-reperfusion injury. Exp Physiol. 2011;96(9):840–6.
9. Calvert JW, Jha S, Gundewar S, Elrod JW, Ramachandran A, Pattillo CB, et al. Hydrogen sulfide mediates cardioprotection through Nrf2 signaling. Circ Res. 2009;105:365–74.
10. Hunter JP, Hosgood SA, Patel M, Rose R, Read K, Nicholson ML. Effects of hydrogen sulphide in an experimental model of renal ischaemia-reperfusion injury. Br J Surg. 2012;99:1665–71.
11. Fu Z, Liu X, Geng B, Fang L, Tang C. Hydrogen sulfide protects rat lung from ischemia-reperfusion injury. Life Sci. 2008;82:1196–202.
12. Henderson PW, Weinstein AL, Sohn AM, Jimenez N, Krijgh DD, Spector JA. Hydrogen sulfide attenuates intestinal ischemia-reperfusion injury when delivered in the post-ischemic period. J Gastroenterol Hepatol. 2010;25:1642–7.

13. Wang D, Ma Y, Li Z, Kang K, Sun X, Pan S, et al. The role of AKT1 and autophagy in the protective effect of hydrogen sulphide against hepatic ischemia/reperfusion injury in mice. Autophagy. 2012;8:954–62.
14. Jha S, Calvert JW, Duranski MR, Ramachandran A, Lefer DJ. Hydrogen sulfide attenuates hepatic ischemia-reperfusion injury: role of antioxidant and antiapoptotic signaling. Am J Physiol Heart Circ Physiol. 2008;295:H801–6.
15. Kang K, Zhao M, Jiang H, Tan G, Pan S, Sun X. Role of hydrogen sulfide in hepatic ischemia-reperfusion-induced injury in rats. Liver Transpl. 2009;15:1306–14.
16. Bos EM, Snijder PM, Jekel H, Weij M, Leemans JC, van Dijk MC, et al. Beneficial effects of gaseous hydrogen sulfide in hepatic ischemia/reperfusion injury. Transpl Int. 2012;25:897–908.
17. Kis A, Yellon DM, Baxter GF. Second window of protection following myocardial preconditioning: an essential role for PI3 kinase and p70S6 kinase. J Mol Cell Cardiol. 2003;35:1063–71.
18. Ban K, Kozar RA. Protective role of p70S6 K in intestinal ischemia/reperfusion injury in mice. PLoS One. 2012;7:e41584.
19. Lowicka E, Beltowski J. Hydrogen sulfide (H2S)—the third gas of interest for pharmacologists. Pharmacological reports. 2007;59:4–24.
20. Fukai M, Hayashi T, Yokota R, Shimamura T, Suzuki T, Taniguchi M, et al. Lipid peroxidation during ischemia depends on ischemia time in warm ischemia and reperfusion of rat liver. Free Radic Biol Med. 2005;38:1372–81.
21. Yadav SS, Gao W, Harland RC, Clavien PA. A new and simple technique of total hepatic ischemia in the mouse. Transplantation. 1998;65:1433–6.
22. Suzuki S, Nakamura S, Koizumi T, Sakaguchi S, Baba S, Muro H, et al. The beneficial effect of a prostaglandin I2 analog on ischemic rat liver. Transplantation. 1991;52:979–83.
23. Szabo C. Hydrogen sulphide and its therapeutic potential. Nat Rev Drug Discov. 2007;6:917–35.
24. Nakamitsu A, Hiyama E, Imamura Y, Matsuura Y, Yokoyama T. Kupffer cell function in ischemic and nonischemic livers after hepatic partial ischemia/reperfusion. Surg Today. 2001;31:140–8.
25. Schlegel A, Graf R, Clavien PA, Dutkowski P. Hypothermic oxygenated perfusion (HOPE) protects from biliary injury in a rodent model of DCD liver transplantation. J Hepatol. 2013;59:984–91.
26. Chen Y, Wood KJ. Interleukin-23 and TH17 cells in transplantation immunity: does 23 + 17 equal rejection? Transplantation. 2007;84:1071–4.
27. Husted TL, Blanchard J, Schuster R, Shen H, Lentsch AB. Potential role for IL-23 in hepatic ischemia/reperfusion injury. Inflamm Res. 2006;55:177–8.
28. Bhogal RH, Weston CJ, Curbishley SM, Adams DH, Afford SC. Activation of CD40 with platelet derived CD154 promotes reactive oxygen species dependent death of human hepatocytes during hypoxia and reoxygenation. PLoS One. 2012;7:e30867.
29. Ke B, Shen XD, Ji H, Kamo N, Gao F, Freitas MC, et al. HO-1-STAT3 axis in mouse liver ischemia/reperfusion injury: regulation of TLR4 innate responses through PI3 K/PTEN signaling. J Hepatol. 2011;56:359–66.
30. Shen X, Wang Y, Gao F, Ren F, Busuttil RW, Kupiec-Weglinski JW, et al. CD4 T cells promote tissue inflammation via CD40 signaling without de novo activation in a murine model of liver ischemia/reperfusion injury. Hepatology. 2009;50:1537–46.
31. Yokota R, Fukai M, Shimamura T, Suzuki T, Watanabe Y, Nagashima K, et al. A novel hydroxyl radical scavenger, nicaraven, protects the liver from warm ischemia and reperfusion injury. Surgery. 2000;127:661–9.
32. Ota T, Hirai R, Urakami A, Soga H, Nawa S, Shimizu N. Endothelin-1 levels in portal venous blood in relation to hepatic tissue microcirculation disturbance and hepatic cell injury after ischemia/reperfusion. Surg Today. 1997;27:313–20.
33. Johansen D, Ytrehus K, Baxter GF. Exogenous hydrogen sulfide (H2S) protects against regional myocardial ischemia-reperfusion injury–Evidence for a role of K ATP channels. Basic Res Cardiol. 2006;101:53–60.
34. Elrod JW, Calvert JW, Morrison J, Doeller JE, Kraus DW, Tao L, et al. Hydrogen sulfide attenuates myocardial ischemia-reperfusion injury by preservation of mitochondrial function. Proc Natl Acad Sci USA. 2007;104:15560–5.
35. Kimura Y, Goto Y, Kimura H. Hydrogen sulfide increases glutathione production and suppresses oxidative stress in mitochondria. Antioxid Redox Signal. 2010;12:1–13.
36. Paine A, Eiz-Vesper B, Blasczyk R, Immenschuh S. Signaling to heme oxygenase-1 and its anti-inflammatory therapeutic potential. Biochem Pharmacol. 2010;80:1895–903.
37. Kim YC, Yamaguchi Y, Kondo N, Masutani H, Yodoi J. Thioredoxin-dependent redox regulation of the antioxidant responsive element (ARE) in electrophile response. Oncogene. 2003;22:1860–5.
38. Akamatsu Y, Haga M, Tyagi S, Yamashita K, Graça-Souza AV, Ollinger R, et al. Heme oxygenase-1-derived carbon monoxide protects hearts from transplant associated ischemia reperfusion injury. Faseb J. 2004;18:771–2.
39. Wei Y, Chen P, de Bruyn M, Zhang W, Bremer E, Helfrich W. Carbon monoxide-releasing molecule-2 (CORM-2) attenuates acute hepatic ischemia reperfusion injury in rats. BMC Gastroenterol. 2010;10:42.
40. Watanabe R, Nakamura H, Masutani H, Yodoi J. Anti-oxidative, anti-cancer and anti-inflammatory actions by thioredoxin 1 and thioredoxin-binding protein-2. Pharmacol Ther. 2010;127:261–70.
41. Shao JL, Wan XH, Chen Y, Bi C, Chen HM, Zhong Y, et al. H_2S protects hippocampal neurons from anoxia-reoxygenation through cAMP-mediated PI3 K/Akt/p70S6 K cell-survival signaling pathways. J Mol Neurosci. 2011;43:453–60.
42. Si R, Tao L, Zhang HF, Yu QJ, Zhang R, Lv AL, et al. Survivin: a novel player in insulin cardioprotection against myocardial ischemia/reperfusion injury. J Mol Cell Cardiol. 2011;50:16–24.
43. Koh PO. Melatonin prevents hepatic injury-induced decrease in Akt downstream targets phosphorylations. J Pineal Res. 2011;51:214–9.
44. Debonera F, Wang G, Xie J, Que X, Gelman A, Leclair C, et al. Severe preservation injury induces Il-6/STAT3 activation with lack of cell cycle progression after partial liver graft transplantation. Am J Transplant. 2004;4:1964–71.
45. Taub R. Liver regeneration: from myth to mechanism. Nat Rev Mol Cell Biol. 2004;5:836–47.
46. Zhang Q, Fu H, Zhang H, Xu F, Zou Z, Liu M, et al. Hydrogen sulfide preconditioning protects rat liver against ischemia/reperfusion injury by activating Akt-GSK-3β signaling and inhibiting mitochondrial permeability transition. PLoS One. 2013;8:e74422.
47. Klingerman CM, Trushin N, Prokopczyk B, Haouzi P. H_2S concentrations in the arterial blood during H_2S administration in relation to its toxicity and effects on breathing. Am J Physiol Regul Integr Comp Physiol. 2013;305:R630–8.
48. Vitvitsky V, Kabil O, Banerjee R. High turnover rates for hydrogen sulfide allow for rapid regulation of its tissue concentrations. Antioxid Redox Signal. 2012;17:22–31.
49. Balaban CL, Rodriguez JV, Guibert EE. Delivery of the bioactive gas hydrogen sulfide during cold preservation of rat liver: effects on hepatic function in an ex vivo model. Artif Organs. 2011;35:508–15.

Cancer Science
Japanese Cancer Association JCA
Open Access

Suprabasin as a novel tumor endothelial cell marker

Mohammad T. Alam,[1,2,6] Hiroko Nagao-Kitamoto,[1,6] Noritaka Ohga,[1] Kosuke Akiyama,[1] Nako Maishi,[1] Taisuke Kawamoto,[1] Nobuo Shinohara,[3] Akinobu Taketomi,[4] Masanobu Shindoh,[2] Yasuhiro Hida[5] and Kyoko Hida[1]

[1]Vascular Biology, Frontier Research Unit, Institute for Genetic Medicine, Hokkaido University, Sapporo; [2]Department of Oral Pathology and Biology, Graduate School of Dental Medicine, Hokkaido University, Sapporo; Departments of [3]Renal and Genitourinary Surgery; [4]Gastroenterological Surgery I; [5]Cardiovascular and Thoracic Surgery, Graduate School of Medicine, Hokkaido University, Sapporo, Japan

Key words

Angiogenesis, suprabasin, suprabasin signaling, tumor endothelial cell marker, tumor endothelial cells

Correspondence

Kyoko Hida, Vascular Biology, Frontier Research Unit, Institute for Genetic Medicine, Hokkaido University, N15, W7, Kita-Ku, Sapporo 060-0815, Japan.
Tel: +81-11-706-4315; Fax: +81-11-706-4325;
E-mail: khida@igm.hokudai.ac.jp

[6]These authors contributed equally to this manuscript.

Funding Information

This article was supported in part by a Grant-in-Aid for scientific research from the Ministry of Education, Science and Culture of Japan (20390506 and 23112501 to Kyoko Hida). The funders had no role in study design, data collection and analysis, decision to publish, or preparation of the manuscript.

Received June 3, 2014; Revised September 26, 2014; Accepted September 30, 2014

Cancer Sci **105** (2014) 1533–1540

doi: 10.1111/cas.12549

Recent studies have reported that stromal cells contribute to tumor progression. We previously demonstrated that tumor endothelial cells (TEC) characteristics were different from those of normal endothelial cells (NEC). Furthermore, we performed gene profile analysis in TEC and NEC, revealing that suprabasin (SBSN) was upregulated in TEC compared with NEC. However, its role in TEC is still unknown. Here we showed that SBSN expression was higher in isolated human and mouse TEC than in NEC. SBSN knockdown inhibited the migration and tube formation ability of TEC. We also showed that the AKT pathway was a downstream factor of SBSN. These findings suggest that SBSN is involved in the angiogenic potential of TEC and may be a novel TEC marker.

Tumor angiogenesis is necessary for the progression of tumor growth and metastasis.[1,2] Because tumor blood vessels supply tumor cells with nutrients and oxygen, anti-angiogenesis treatment is recognized as a new cancer therapy.[3] Bevacizumab, anti-vascular endothelial growth factor (VEGF) antibody,[4] and sorafenib or sunitinib, a VEGF receptor kinase inhibitor, have been used as anti-angiogenic drugs.[5] However, there are negative reports regarding side effects and increases in metastasis have been observed. To overcome these problems, a new anti-angiogenic drug is required.[6] The morphology of tumor blood vessels is different from that of normal blood vessels.[7–9] Differences between tumor endothelial cells (TEC) and normal endothelial cells (NEC) in aspects, such as gene expression and biological behavior, have also been reported.[7,8,10] Recently, we revealed that TEC were more resistant to anti-cancer drugs compared with NEC.[11] In addition, inhibition of cyclooxygenase-2 or lysyl oxidase in TEC suppressed tumor growth and lung metastasis *in vivo*.[12,13] These findings indicate that TEC may be a good target for anti-cancer therapy. To identify specific TEC markers, we performed DNA microarray analysis and reported that some molecules were upregulated in TEC.[14–16] Among these molecules, suprabasin (SBSN) showed very high expression levels in several TEC.

Suprabasin has been identified as an epidermal differentiation marker and has been detected in the suprabasal layers of the epithelia in the epidermis, stomach and tongue in mice.[17,18] SBSN participates in the proliferation of normal small cell lung carcinoma cells.[19] The SBSN expression is also correlated with the growth and invasiveness of salivary gland adenoid cystic carcinoma and glioblastoma.[20,21] However, the details of SBSN's involvement in tumor malignancy and tumor angiogenesis are unknown.

In this study, we examined the SBSN expression and its function in TEC to determine whether SBSN is a potential TEC marker.

Materials and Methods

Cell lines and culture conditions. The human renal clear cell carcinoma cell OS-RC-2 was purchased from the RIKEN Cell Bank (Tsukuba, Japan) and cultured in RPMI1640 medium (Sigma–Aldrich, St. Louis, MO, USA) supplemented with 10% heat-inactivated FBS, 100 U/mL penicillin and 100 μg/mL streptomycin. A375SM cells, a super-metastatic human melanoma cell line, were a gift from Dr Isaiah J Fidler (MD Anderson Cancer Center, Houston, TX, USA). The cells were cultured in minimum essential medium (Gibco, Grand Island, NY, USA) supplemented with 10% FBS, 100 U/mL penicillin and 100 μg/mL

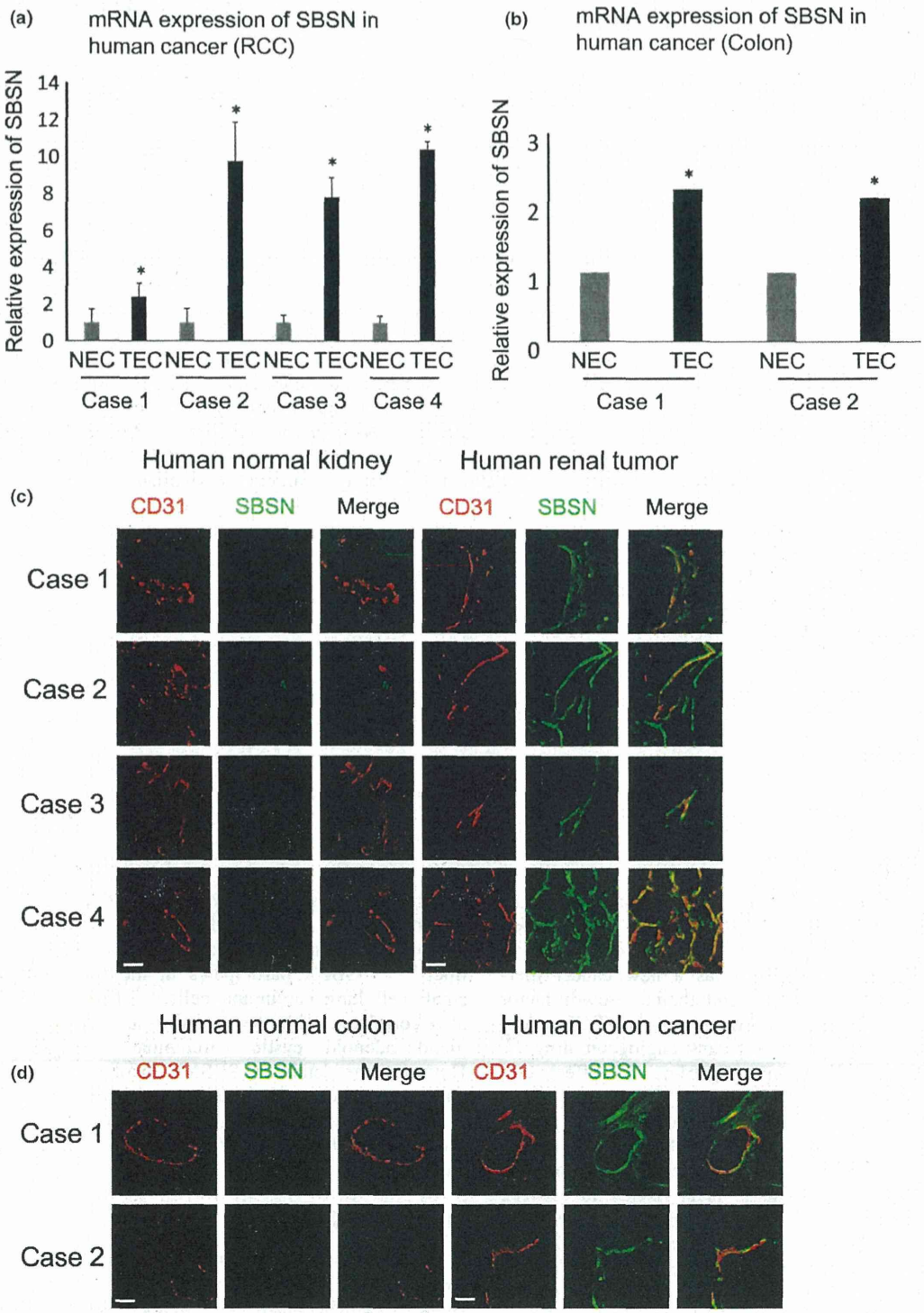

Fig. 1. Suprabasin (SBSN) expression in human tumor endothelial cells (hTEC). (a, b) Relative *SBSN* mRNA expression levels in hNEC and hTEC evaluated by quantitative PCR (a, RCC, $n = 4$; b, colon tumor, $n = 2$). *$P < 0.01$ versus control; two-sided Student's *t*-test. (c, d) Clinical samples of renal cell carcinoma (RCC) and colon cancer-derived tumor endothelial cells were double-stained with anti-CD31 and anti-SBSN antibodies. Scale bar: 50 μm.

streptomycin, as described previously.[15] In the growth factor experiments, NEC were treated with human EGF (AF-100-15; PeproTech, Rocky Hill, NJ, USA) at final concentrations of 5 and 15 ng/mL and human VEGF (100-20; PeproTech, Rocky Hill, NJ, USA) at final concentrations of 15 and 30 ng/mL for 12 h. These cells were cultured at 37°C in a humidified atmosphere of 5% CO_2 and 95% air.

Isolation of tumor endothelial cells and normal endothelial cells. All procedures for animal experiments were approved by the local animal research authorities, and animal care

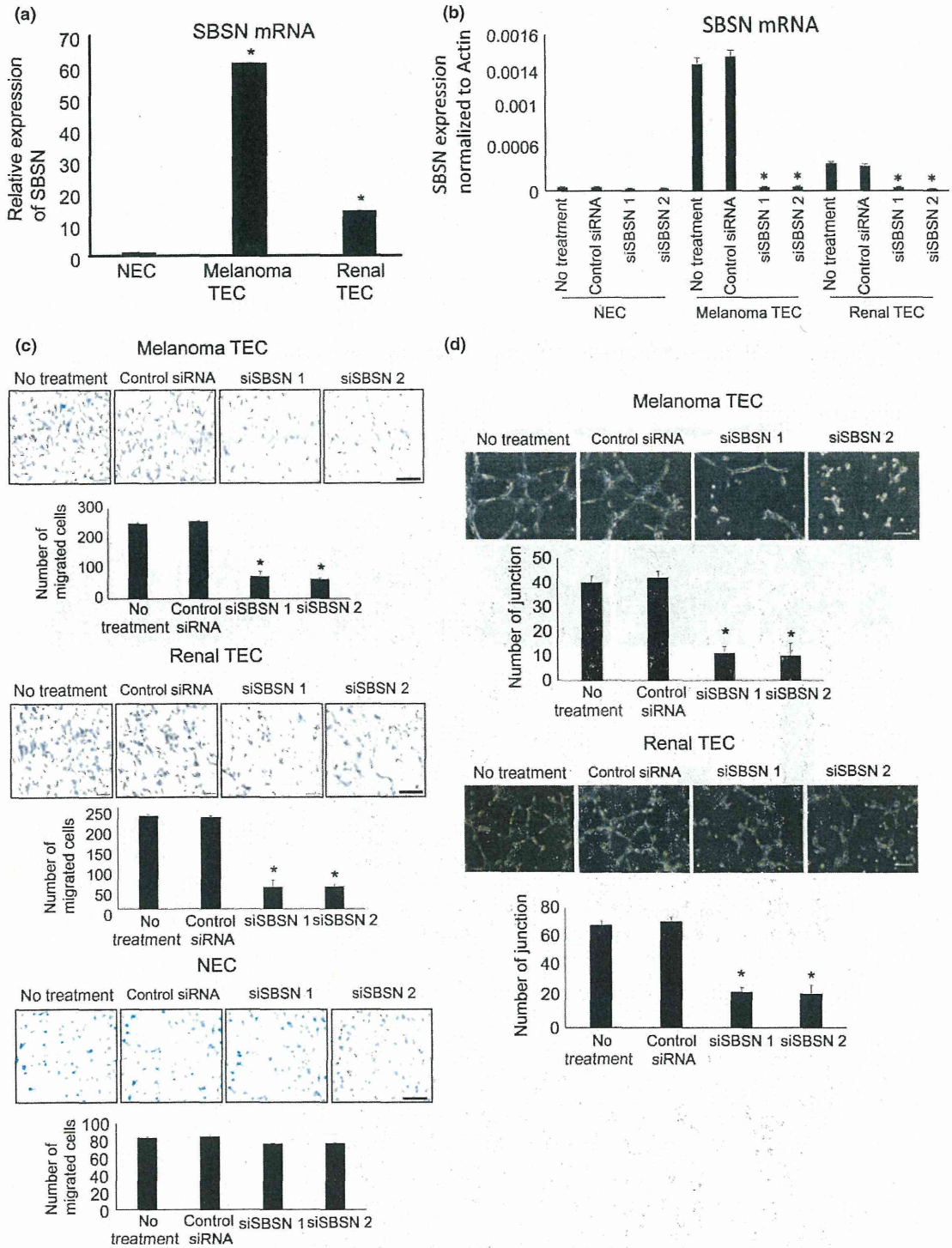

Fig. 2. Effect of *SBSN* knockdown on cell migration and tube formation in mouse tumor endothelial cells (mTEC). (a) Relative *SBSN* mRNA expression levels in mouse normal endothelial cells (mNEC) and mTEC (melanoma and renal) evaluated by quantitative PCR. (b) *SBSN* mRNA expression levels in mTEC and mNEC transfected with the control siRNA or si*SBSN*, determined by quantitative PCR. (c) Migration toward vascular endothelial growth factor (VEGF) of mTEC and mNEC transfected with control siRNA or si*SBSN* analyzed using a Boyden chamber. Scale bar: 100 μm. (d) Tube number of mTEC transfected with control siRNA or si*SBSN*. Scale bar: 50 μm. $*P < 0.01$ versus control; one-way ANOVA with the Tukey–Kramer multiple comparison test (mean ± SD, $n = 3$).

was performed in accordance with institutional guidelines. Mouse TEC (mTEC) and NEC (mNEC) were isolated as previously described[12] with some modifications. Diphtheria toxin (500 ng/mL; Calbiochem, San Diego, CA, USA) was added to mTEC subcultures to kill any human tumor cells and to mNEC subcultures for technical consistency. Using

an anti-human CD31 antibody, human TEC (hTEC) and NEC (hNEC) were isolated from excised renal cell carcinoma (RCC) or colon cancer tissues from patients at Hokkaido University Hospital. Normal renal or colon tissues were obtained from areas that were adjacent to the tumor in the same patient. Clinical background information is described

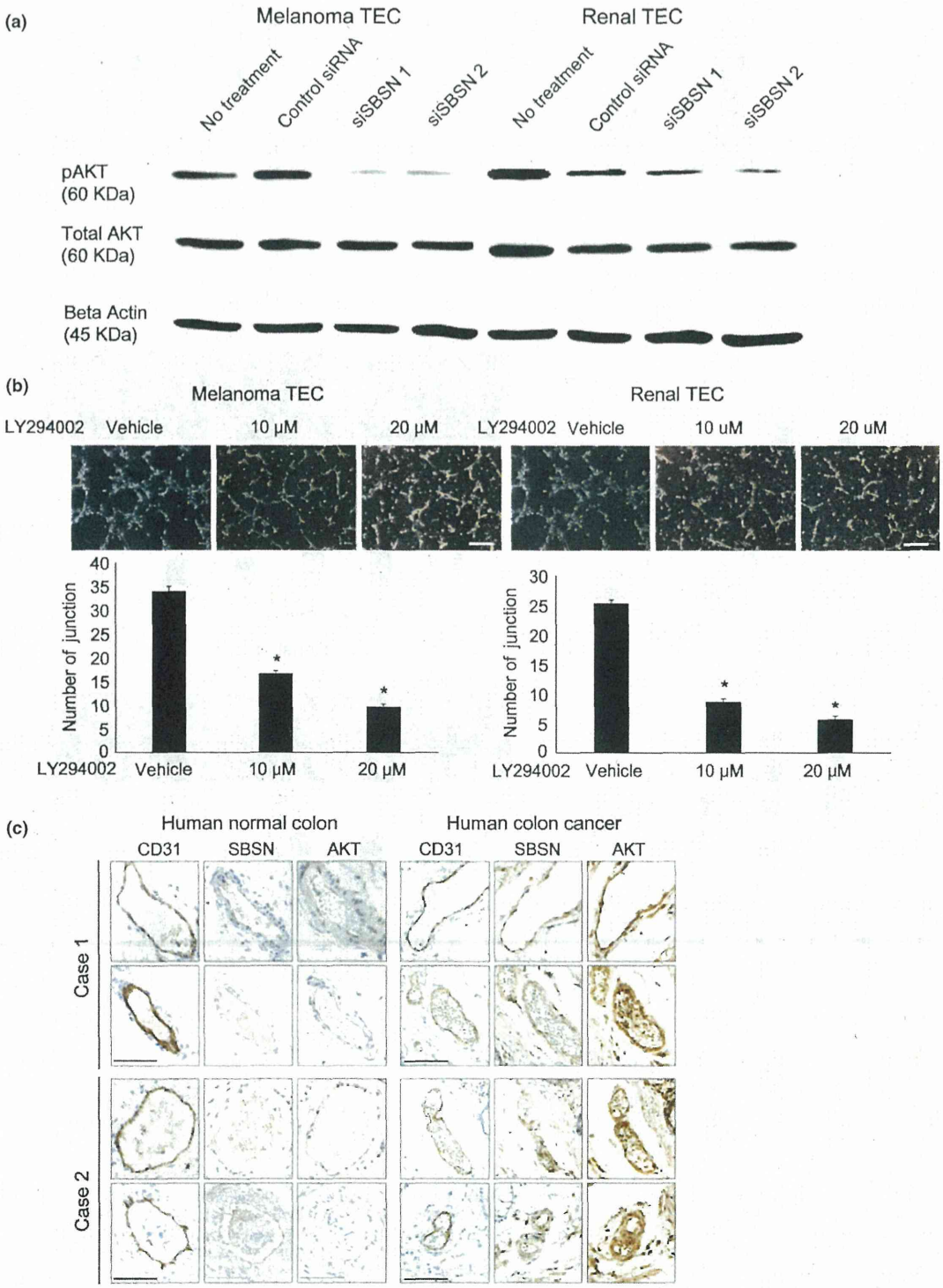

Fig. 3. Relationship between suprabasin (SBSN) knockdown and AKT activation in mouse tumor endothelial cells (mTEC) *in vitro* and *in vivo*. (a) Total AKT, phosphorylated AKT (p-AKT), and beta actin protein levels in mTEC treated with control siRNA or si*SBSN*, determined by western blotting. (b) Tube number of mTEC treated with or without LY294002 (10 or 20 μM) evaluated by the tube formation assay. Scale bar: 100 μm. *$P < 0.05$ versus control; two-sided Student's *t*-test (mean ± SD, $n = 3$). (c) SBSN and AKT expression levels were determined by immunohistochemical analysis. CD31-positive blood vessels were stained with anti-SBSN and anti-AKT antibodies in two cases of human colon cancer (Cases 1 and 2), whereas those of normal tissues were weakly stained *in vivo*. Scale bar: 80 μm.

in Supplementary Table S1. These protocols were approved by the Ethics Committee of Hokkaido University, and written informed consent was obtained from each patient before surgery. Endothelial cells (EC) were cultured as previously described.[22,23]

Reverse transcription and quantitative PCR. Total RNA was extracted from cells and human tumor and normal tissue samples using the ReliaPrep RNA Cell Miniprep System (Promega Corporation, Madison, WI, USA). Complementary DNA (cDNA) was synthesized using a ReverTra-Plus kit (Toyobo, Osaka, Japan). For relative quantification of target mRNA, we used SsoFast EvaGreen Supermix (CFX 96 Real-Time PCR Detection System; Bio-Rad, Hercules, CA, USA) for mouse EC and SYBR Green Real-time PCR Master Mix-Plus (Bio-Rad) for human EC (in triplicate) according to the manufacturer's instructions.[24] The quantitative PCR amplification program was performed at 95°C for 3 min and 45 cycles at 95°C for 10 s and 60°C for 30 s. Data were analyzed with CFX Manager software (Bio-Rad). The primers used are described in Supplementary Table S2. Each experiment included four PCR reactions, and each experiment was performed three times.

Western blotting. Western blotting analysis was performed as described previously.[25] This analysis used antibodies specific for total AKT, phosphorylated AKT (Cell Signaling Technology, Beverly, MA, USA), total Erk, phosphorylated Erk (Cell Signaling Technology), beta actin and an HRP-conjugated secondary antibody.

Immunostaining. Human tissue samples were obtained from excised RCC, normal renal tissue, colon cancer and normal colon tissues of patients at Hokkaido University Hospital. Frozen sections of excised tissues were prepared as previously described.[14,26] Human sections were double-stained with anti-human CD31/Alexa Fluor 594 rat anti-mouse IgG and anti-SBSN/Alexa Fluor 488 goat anti-rabbit IgG. All samples were counterstained with DAPI (Roche Diagnostics, Mannheim, Germany) and examined using an Olympus FluoView FV10i confocal microscope (Olympus, Tokyo, Japan).

For AKT staining, formalin-fixed paraffin-embedded specimens from two cases of colon cancer were prepared. Immunohistochemical analysis was performed using serial sections that were stained with anti-SBSN (1:250 dilution), AKT (1:100 dilution) and CD31 (Leica Microsystem, UK; 1:500 dilution), followed by antibody detection using a peroxidase-conjugated streptavidin-diaminobenzidine (DAB) readout system (DAKO), and counterstaining with DAPI. Images were randomly captured using a nanozoomer slide scanner and NDPViewer (Hamamatsu, Japan).

Suprabasin knockdown. si*SBSN* was transfected into cells using Lipofectamine transfection reagent (Invitrogen, Tokyo, Japan) according to the manufacturer's instructions. The sequence of si*SBSN* was 5′-UAUUGAUGCCUUCAA GGGCCUUGCC-3′ (siSBSN1) and 5′-UUCCCUUCCAGCU UGAGUGAUUCCG-3′ (siSBSN2). A nontargeting control siRNA was used (Invitrogen).

Cell migration assay. Cell migration toward VEGF-A was analyzed using a Boyden chamber (Neuro Probe, Gaithersburg, MD, USA), as previously described.[27] VEGF-A (10 ng/mL) was added to the lower chamber as a chemoattractant. TEC were treated with the control siRNA (10 nM) or si*SBSN* (10 nM) in endothelial basal medium (EBM)-2 supplemented with 0.5% FBS for 24 h. In total, 1.5×10^4cells were seeded in the upper chamber and incubated for 4 h at 37°C. The assays were independently performed three times.

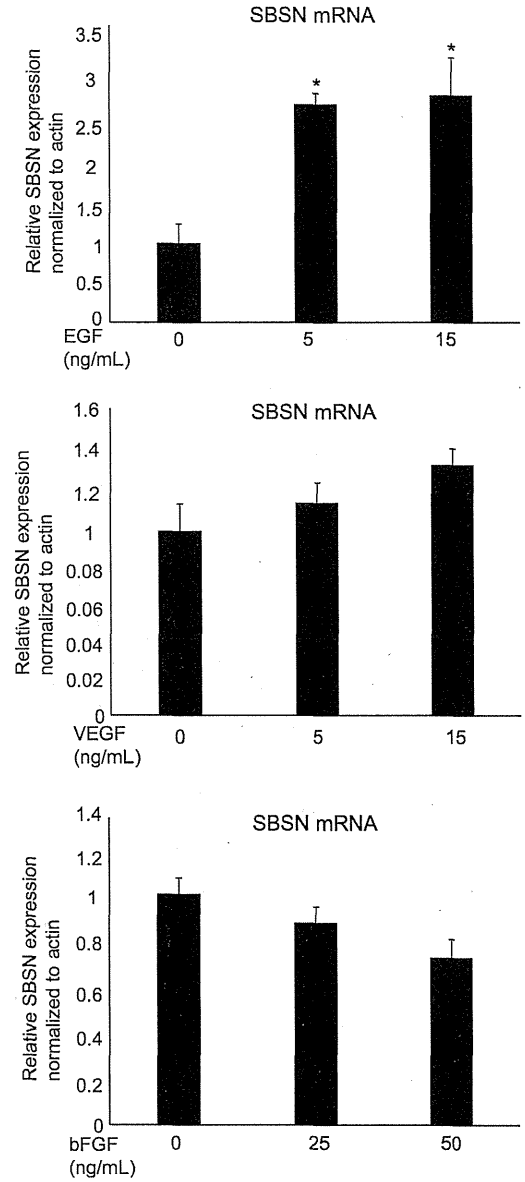

Fig. 4. Suprabasin (SBSN) expression after growth factor treatment. NEC were incubated in 0.5% EBM2 medium for 12 h, followed by treatment with endothelial growth factor (EGF), vascular endothelial growth factor (VEGF) and basic fibroblast growth factor (bFGF) for 12 h. The cells were cultured at 37°C in a humidified atmosphere of 5% CO_2. *$P < 0.05$ versus control; two-sided student's *t*-test. After 12 h of incubation, mRNA was extracted from the cells and used in the RT-PCR analysis of SBSN expression.

Tube formation assay. A tube formation assay was performed as previously described.[26] EC were seeded at a density of 1.0×10^5 cells per well and incubated at 37°C on Matrigel (BD Biosciences, San Jose, CA, USA). Tube formation was observed using an inverted microscope by measuring the junction number of endothelial tubes. For inhibition experiments using the PI3 kinase inhibitor LY294002, TEC were preincubated for 2 h at 37°C in EBM2 supplemented with 0.5% FBS. To investigate the involvement of AKT in TEC tube formation, assays were performed with or without LY294002 (0, 10

or 20 μM). The assays were independently performed three times.

Cell proliferation assay. Cell proliferation was assessed with an MTS assay as described previously.[11] TEC were treated with the control siRNA (10 nM) or si*SBSN* (10 nM) in EBM2 supplemented with 0.5% FBS for 24 h. After siRNA transfection, 1.0×10^3 cells per well were seeded into 96-well plates in EBM2 supplemented with 5% FBS. Cell proliferation was measured daily for 3 days by the MTS assay. The assays were independently performed three times.

Statistical analysis. Results are given as mean ± SD. Group comparisons were made by one-way ANOVA with the Tukey–Kramer multiple comparison test. When only two groups were compared, a two-sided Student's *t*-test was used. $P < 0.05$ was considered significant, and $P < 0.01$ was considered highly significant.

Results

Suprabasin was highly expressed in human tumor endothelial cells. To analyze the SBSN expression in hTEC and hNEC, we isolated hTEC from tissues of four cases of RCC and two cases of colon cancer. Furthermore, hNEC were isolated from the tissues of normal renal tissue and colon in the same patients.[14,28] The *SBSN* mRNA expression levels in hTEC isolated from RCC and colon cancer tissues were higher than those of hNEC (Fig. 1a,b). Double-immunofluorescence staining with anti-SBSN and anti-CD31 antibodies revealed that SBSN was markedly expressed in tumor blood vessels both in RCC and colon cancer, whereas the SBSN expression was low in normal blood vessels (Fig. 1c,d). In addition, SBSN mRNA expression levels were higher in human renal tumor tissues than those in normal tissues (Suppl. Fig. S1). These findings showed that SBSN was upregulated in hTEC from several tumor types.

Suprabasin knockdown inhibited migration and tube formation of mouse tumor endothelial cells. To clarify the role of SBSN in TEC, we used mTEC isolated from human tumor xenografts (A375SM and OS-RC-2). mNEC were isolated from mouse dermis as a normal control. We verified that mNEC and mTEC had the characteristics of EC using an RT-PCR assay (Suppl. Fig. S2). The *SBSN* mRNA expression levels were upregulated in mTEC from melanoma and renal carcinoma compared with mNEC (Fig. 2a) and other mouse normal tissues (Suppl. Fig. S3). To evaluate the SBSN function in TEC, we examined the migration ability and tube formation of mTEC following the *SBSN* knockdown. The efficacy of RNA interference (RNAi) was confirmed using quantitative real-time PCR, which showed that si*SBSN*, unlike control siRNA, decreased the SBSN mRNA level in mTEC and mNEC (Fig. 2b). We next demonstrated that the *SBSN* knockdown significantly suppressed cell migration toward VEGF-A in mTEC but not in mNEC (Fig. 2c). However, siSBSN had no effect on cell proliferation in either mTEC or mNEC (Suppl. Fig. S4). In this study, we used two types of siRNA and obtained similar results. This suggests that the results are not off-target effects of the nucleic acids. In addition, the junction number of endothelial tubes in mTEC was reduced by si*SBSN* treatment (Fig. 2d). These findings revealed that SBSN contributed to the angiogenic phenotype, such as migration and tube formation in mTEC.

Suprabasin knockdown suppressed AKT pathway in mouse tumor endothelial cells. The PI3K/AKT pathway plays an essential role in the survival of TEC.[29] We previously reported that activation of AKT was involved in cell migration of mTEC;[13,23] and, therefore, we explored the interaction between the AKT pathway and SBSN. Phosphorylation of AKT in mTEC was suppressed by the PI3K inhibitor LY294002 treatment (Suppl. Fig. S5a). Moreover, we showed that the protein level of phosphorylated AKT was reduced by si*SBSN* treatment compared with control siRNA in both types of mTEC (melanoma and renal) (Fig. 3a), but not in NEC or in other cell types (Suppl. Fig. S5b). Moreover, we demonstrated that LY294002 inhibited tube formation in mTEC in a concentration-dependent manner (Fig. 3b). These findings indicate that SBSN regulated the migration and tube formation of mTEC via the AKT pathway. In addition, SBSN-positive blood vessels in human colon cancer tissues were positively stained by anti-AKT, but not those of normal colon tissues (Fig. 3c). This result suggests that SBSN may also be involved in AKT activation in human tumor blood vessels. To address how SBSN expression is regulated, endothelial cells were treated with growth factors such as endothelial growth factor (EGF), VEGF and fibroblast growth factor-2 (FGF-2). Among these growth factors, EGF significantly induced SBSN mRNA expression in NEC (Fig. 4).

Discussion

In this study, we demonstrated that the SBSN expression was markedly increased in human TEC (renal carcinoma and colon carcinomas) as well as mTEC (melanoma and renal carcinoma). These findings indicate that SBSN may be used as a common marker of TEC.

The *SBSN* mRNA expression levels tended to be higher in hTEC (isolated from renal carcinoma) with higher T classifications under the tumor-node-metastasis system (order: case 4 > 2 > 3 > 1) (Suppl. Table S1). In this study, because the number of clinical samples was small, further studies are required to explore the relationship between the SBSN expression and clinical background in larger numbers of patients.

Previously, we reported that mTEC demonstrate a pro-angiogenic phenotype compared with mNEC.[11,30,31] SBSN plays a role in epidermal differentiation[18] and the growth and invasiveness of tumors.[19–21] For example, Shao *et al.*[21] report that SBSN was upregulated because the SBSN gene promoter in adenocystic carcinoma was demethylated. However, our preliminary analysis of epigenetics showed that methylation levels in TEC did not differ from those in NEC, which suggests that there may be another mechanism that is responsible for the enhanced expression of the *SBSN* gene in TEC. We found that EGF upregulated the expression of SBSN in NEC. However, its mechanism of transcriptional regulation or its function in tumor angiogenesis is unknown. In this study, we demonstrated that the *SBSN* knockdown inhibited cell migration and tube formation in mTEC. These findings revealed the role of SBSN in tumor angiogenesis.

We previously reported that the VEGF receptor-2 (VEGFR-2) expression was high in TEC and that TEC were more sensitive to VEGF than NEC.[27] The *SBSN* knockdown had no significant effect on the *VEGFR* mRNA expression in mTEC, suggesting that involvement of SBSN in the angiogenic phenotype of mTEC is independent of VEGF/VEGFR-2 signaling.

There has been no report of SBSN signaling. We showed that the activation of AKT was suppressed by siSBSN. However, activation of the ERK pathway, which is related to angiogenesis, was not affected (Suppl. Fig. S6). Our finding revealed at least a part of downstream signaling of SBSN in TEC. Thus, these findings enhanced our understanding of TEC function.

Our data demonstrate that the number of tube junctions in TEC was decreased more by si*SBSN* than by a PI3K inhibitor.

These results suggest that other molecules besides AKT are involved in SBSN-related tube formation in mTEC. Additional studies are required to determine whether the AKT is directly involved in the downstream of SBSN.

In this study, to the best of our knowledge, we demonstrated for the first time that SBSN is upregulated in TEC and that SBSN plays significant roles in the pro-angiogenic phenotype in TEC, but not in NEC. In this study, we showed that SBSN could be a potential TEC marker. Thus, SBSN may be a novel target for anti-angiogenic therapy, which is specific for tumor blood vessels.

Acknowledgments

We thank Dr I. J. Fidler for providing the A375SM super-metastatic human malignant melanoma cell line and Dr Aya Matsuda, Ms. Yuko Suzuki, and Ms. Tomomi Takahashi for their technical assistance in the experiments. This article was supported in part by a Grant-in-Aid for scientific research from the Ministry of Education, Science and Culture of Japan (20390506 and 23112501 to Kyoko Hida). The funders had no role in study design, data collection and analysis, decision to publish, or preparation of the manuscript.

Disclosure Statement

The authors have no conflict of interest to declare.

References

1 Folkman J. Role of angiogenesis in tumor growth and metastasis. *Semin Oncol* 2002; **29**: 15–8.
2 Folkman J. Angiogenesis: an organizing principle for drug discovery? *Nat Rev Drug Discov* 2007; **6**: 273–86.
3 Welti J, Loges S, Dimmeler S, Carmeliet P. Recent molecular discoveries in angiogenesis and antiangiogenic therapies in cancer. *J Clin Invest* 2013; **123**: 3190–200.
4 Willett CG, Boucher Y, di Tomaso E *et al.* Direct evidence that the VEGF-specific antibody bevacizumab has antivascular effects in human rectal cancer. *Nat Med* 2004; **10**: 145–7.
5 Ivy SP, Wick JY, Kaufman BM. An overview of small-molecule inhibitors of VEGFR signaling. *Nat Rev Clin Oncol* 2009; **6**: 569–79.
6 Jain RK, Duda DG, Clark JW, Loeffler JS. Lessons from phase III clinical trials on anti-VEGF therapy for cancer. *Nat Clin Pract Oncol* 2006; **3**: 24–40.
7 McDonald DM, Baluk P. Significance of blood vessel leakiness in cancer. *Cancer Res* 2002; **62**: 5381–5.
8 Morikawa S, Baluk P, Kaidoh T, Haskell A, Jain RK, McDonald DM. Abnormalities in pericytes on blood vessels and endothelial sprouts in tumors. *Am J Pathol* 2002; **160**: 985–1000.
9 Jain RK. Molecular regulation of vessel maturation. *Nat Med* 2003; **9**: 685–93.
10 St Croix B, Rago C, Velculescu V *et al.* Genes expressed in human tumor endothelium. *Science* 2000; **289**: 1197–202.
11 Akiyama K, Ohga N, Hida Y *et al.* Tumor endothelial cells acquire drug resistance by MDR1 up-regulation via VEGF signaling in tumor microenvironment. *Am J Pathol* 2012; **180**: 1283–93.
12 Osawa T, Ohga N, Akiyama K *et al.* Lysyl oxidase secreted by tumour endothelial cells promotes angiogenesis and metastasis. *Br J Cancer* 2013; **109**: 2237–47.
13 Muraki C, Ohga N, Hida Y *et al.* Cyclooxygenase-2 inhibition causes antiangiogenic effects on tumor endothelial and vascular progenitor cells. *Int J Cancer* 2012; **130**: 59–70.
14 Maishi N, Ohga N, Hida Y *et al.* CXCR7: a novel tumor endothelial marker in renal cell carcinoma. *Pathol Int* 2012; **62**: 309–17.
15 Osawa T, Ohga N, Hida Y *et al.* Prostacyclin receptor in tumor endothelial cells promotes angiogenesis in an autocrine manner. *Cancer Sci* 2012; **103**: 1038–44.
16 Yamamoto K, Ohga N, Hida Y *et al.* Biglycan is a specific marker and an autocrine angiogenic factor of tumour endothelial cells. *Br J Cancer* 2012; **106**: 1214–23.
17 Matsui T, Hayashi-Kisumi F, Kinoshita Y *et al.* Identification of novel keratinocyte-secreted peptides dermokine-alpha/-beta and a new stratified epithelium-secreted protein gene complex on human chromosome 19q13.1. *Genomics* 2004; **84**: 384–97.
18 Park GT, Lim SE, Jang SI, Morasso MI. Suprabasin, a novel epidermal differentiation marker and potential cornified envelope precursor. *J Biol Chem* 2002; **277**: 45195–202.
19 Glazer CA, Smith IM, Ochs MF *et al.* Integrative discovery of epigenetically derepressed cancer testis antigens in NSCLC. *PLoS ONE* 2009; **4**: e8189.
20 Formolo CA, Williams R, Gordish-Dressman H, MacDonald TJ, Lee NH, Hathout Y. Secretome signature of invasive glioblastoma multiforme. *J Proteome Res* 2011; **10**: 3149–59.
21 Shao C, Tan M, Bishop JA *et al.* Suprabasin is hypomethylated and associated with metastasis in salivary adenoid cystic carcinoma. *PLoS ONE* 2012; **7**: e48582.
22 Akino T, Hida K, Hida Y *et al.* Cytogenetic abnormalities of tumor-associated endothelial cells in human malignant tumors. *Am J Pathol* 2009; **175**: 2657–67.
23 Ohga N, Hida K, Hida Y *et al.* Inhibitory effects of epigallocatechin-3 gallate, a polyphenol in green tea, on tumor-associated endothelial cells and endothelial progenitor cells. *Cancer Sci* 2009; **100**: 1963–70.
24 Kondoh M, Ohga N, Akiyama K *et al.* Hypoxia-induced reactive oxygen species cause chromosomal abnormalities in endothelial cells in the tumor microenvironment. *PLoS ONE* 2013; **8**: e80349.
25 Kawamoto T, Ohga N, Akiyama K *et al.* Tumor-derived microvesicles induce proangiogenic phenotype in endothelial cells via endocytosis. *PLoS ONE* 2012; **7**: e34045.
26 Kurosu T, Ohga N, Hida Y *et al.* HuR keeps an angiogenic switch on by stabilising mRNA of VEGF and COX-2 in tumour endothelium. *Br J Cancer* 2011; **104**: 819–29.
27 Matsuda K, Ohga N, Hida Y *et al.* Isolated tumor endothelial cells maintain specific character during long-term culture. *Biochem Biophys Res Commun* 2010; **394**: 947–54.
28 Akiyama K, Ohga N, Maishi N *et al.* The F-prostaglandin receptor is a novel marker for tumor endothelial cells in renal cell carcinoma. *Pathol Int* 2013; **63**: 37–44.
29 Bussolati B, Deambrosis I, Russo S, Deregibus MC, Camussi G. Altered angiogenesis and survival in human tumor-derived endothelial cells. *FASEB J* 2003; **17**: 1159–61.
30 Hida K, Hida Y, Amin DN *et al.* Tumor-associated endothelial cells with cytogenetic abnormalities. *Cancer Res* 2004; **64**: 8249–55.
31 Ohga N, Ishikawa S, Maishi N *et al.* Heterogeneity of tumor endothelial cells: comparison between tumor endothelial cells isolated from high- and low-metastatic tumors. *Am J Pathol* 2012; **180**: 1294–307.

Supporting Information

Additional supporting information may be found in the online version of this article:

Fig. S1. Suprabasin (SBSN) expression in human tumor tissues. Relative *SBSN* mRNA expression levels in both human colon normal and cancer tissues were analyzed by quantitative RT-PCR. $*P < 0.05$ versus control; two-sided Student's *t*-test. Clinical samples from three patients were collected.

Fig. S2. Characterization of isolated mouse tumor endothelial cells (mTEC) and mouse normal endothelial cells (mNEC). mRNA levels of CD31, CD105, VEGFR-1 (VR1), VEGFR-2 (VR2), CD11b, CD45, human HB-EGF (hHB-EGF) and GAPDH in mTEC and mNEC were evaluated by RT-PCR.

Fig. S3. SBSN expression in mouse tumor endothelial cells (mTEC) and other various tissue of mouse organs. Relative *SBSN* mRNA expression levels in various tissue of mouse organs besides ECs analyzed by quantitative PCR. $*P < 0.01$ versus control. (ND, not detected.)

Fig. S4. Effect of si*SBSN* on proliferation of mouse tumor endothelial cells (mTEC) transfected with control siRNA or si*SBSN* was analyzed using the MTS assay.

Fig. S5. (a) Effect of LY294002 treatment on mouse tumor endothelial cells (mTEC). (a) Total AKT, phosphorylated AKT (p-AKT), and beta actin protein levels in mTEC treated or not treated with LY294002 (10 or 20 μM) were determined by western blotting. (b) Total AKT, phosphorylated AKT (p-AKT), and beta actin protein levels in mTEC were compared with those of the NEC, NIH3T3 and B16F10 cell lines transfected with control siRNA or si*SBSN*. Approximately 20 μg of total protein was loaded into each lane for western blot analysis.

Fig. S6. Effect of ERK activation by suprabasin (SBSN) knockdown. ERK activation was determined by western blot analysis. Total ERK and phosphorylated ERK (p-ERK) protein expression levels were detected in mouse tumor endothelial cells (mTEC) transfected with control siRNA or si*SBSN* in melanoma tumor endothelial cells (TEC) and renal TEC. Approximately 20 μg of total protein was loaded into each lane for western blot analysis. Beta actin antibody was used as internal control.

Table S1. Clinical background of renal cell carcinoma (RCC) and colon cancer specimens. M/F, male/female; †according to 1997 tumor-node-metastasis (TNM) staging guidelines; ††according to the Fuhrman system.

Table S2. List of primers. Primer sequences for RT-PCR and quantitative PCR.

Mizukami et al. BMC Cancer 2014, 14:687
http://www.biomedcentral.com/1471-2407/14/687

BMC Cancer

RESEARCH ARTICLE Open Access

Immunohistochemical analysis of cancer stem cell markers in pancreatic adenocarcinoma patients after neoadjuvant chemoradiotherapy

Tatsuzo Mizukami[1†], Hirofumi Kamachi[1*], Tomoko Mitsuhashi[2†], Yosuke Tsuruga[1†], Yutaka Hatanaka[2†], Toshiya Kamiyama[1†], Yoshihiro Matsuno[2†] and Akinobu Taketomi[1†]

Abstract

Background: Cancer stem cells (CSCs) have been reported to play an important role in chemoradiation resistance. Although the association of CSC markers with clinicopathological outcomes after neoadjuvant chemoradiotherapy (NACRT) has been reported in various types of cancers, there have been no such reports for pancreatic cancer. Here we examined the sequential changes in CSC marker expressions after NACRT in patients with pancreatic adenocarcinoma (PA) and the impact of these changes on the prognosis.

Methods: We used immunohistochemistry to evaluate the expressions of the CSC markers epithelial cell adhesion molecule (EpCAM), CD24, CD44, CD133, CXCR4 and Aldehyde dehydrogenase 1 (ALDH1) in resected specimens obtained from 28 PA patients, and we compared these expressions with the patients' clinicopathological parameters and survival data.

Results: The expression frequencies of CD44 and ALDH1 were significantly higher in the NACRT group (n = 17) compared to the non-NACRT group (n = 11), but the CD133 expression was significantly lower in the NACRT group. In the NACRT group, the expression of CD133 was inversely correlated with that of ALDH1, and CD133 +/ALDH1− expression was associated with an unfavorable patient outcome.

Conclusion: This is the first report showing that NACRT may influence the expression frequencies of CD44, CD133 and ALDH1 in PA patients. Moreover, CD133 and ALDH1 expressions may be useful predictors of prognosis in PA patients who have received NACRT.

Keywords: Cancer stem cells, EpCAM, CD24, CD44, CD133, CXCR4, ALDH1, Neoadjuvant chemoradiotherapy, Pancreatic cancer

Background

Pancreatic cancer is the fourth leading cause of cancer death in the United States, and its 5-year survival rate is only 6% [1]. Surgical resection remains the only potentially curative therapeutic option. However, pancreatic cancer proceeds asymptomatically in many cases, and surgical resection is feasible in only 10% to 20% of patients at the time of initial diagnosis [2]. Even after complete resection, the long-term survival rate remains very poor [3,4].

New therapeutic strategies are thus needed to improve the prognosis of pancreatic cancer patients. During the past decade, neoadjuvant chemoradiotherapy (NACRT) for locally advanced pancreatic adenocarcinoma has received attention [5]. NACRT has several positive aspects such as an increased resectability rate with clear margins and decreased rates of metastatic lymph nodes and local relapse, and NACRT resulted in a significant improvement of the 5-year survival rate in curative cases [6,7]. However, many patients with pancreatic cancer do not respond to NACRT, and little is known about the potential

* Correspondence: hkamachi@db3.so-net.ne.jp
†Equal contributors
[1]Department of Gastroenterological Surgery I, Graduate School of Medicine, Hokkaido University, North 15, West 7, Kita-ku, Sapporo 060-8638, Japan
Full list of author information is available at the end of the article

biological markers that may be associated with response to NACRT.

Evidence has accumulated indicating that many solid tumours are driven and managed by rare subpopulations of cancer stem cells (CSCs). In pancreatic cancer, several markers have been used to identify CSCs, such as epithelial cell adhesion molecule (EpCAM, also known as epithelial-specific antigen, or ESA) [8], CD24 [9], CD44 [10,11], CD133 [12,13], CXCR4 [14], aldehyde dehydrogenase 1 (ALDH1) [15,16] and combinations of these markers [17-19]. And it has been reported that the expression of CSCs related to patients prognosis [20]. The biological roles of each CSCs marker are widely different. EpCAM is considered an adhesion molecule. CD24 and CD44 also function as adhesion molecules. CD133 is a cell surface glycoprotein. CXCR4 functions as a chemokine receptor. ALDH1 is an intracellular enzyme involved in retinoic acid.

CSCs seem to be primarily responsible for the frequently observed failure of therapies as well as for relapse after anticancer treatment [21]. In fact, there are several reports of the resistance of CSCs to chemoradiation therapy in head-neck [22], esophageal [23,24], lung [25] and colon [26] cancer, but there has been no report on pancreatic CSCs related to chemoradiation resistance, to our knowledge.

In the present study therefore, we investigated the properties of pancreatic CSCs to compare the expressions of CSC markers in the tumours of PA patients according to whether they received NACRT, and to analyze the associations between the expressions of the CSC markers and the clinicopathological characteristics of the NACRT group to determine the clinical implications of the CSC marker expressions.

Methods

Patient demographics

Between May 2003 and September 2013, 28 PA patients (14 males, 14 females) underwent surgery at the Department of General Surgery I, Hokkaido University Graduate School of Medicine (Sapporo, Japan). Among them, 17 patients received preoperative chemoradiotherapy with gemcitabine (GEM) followed by 50.4 Grays (Gy) of radiation therapy (NACRT group). All patients in the NACRT group received a cumulative irradiation dose of 50.4 Gy in 28 fractions of 1.8 Gy, using 3-dimensional radiation therapy. The primary tumour plus regional lymph nodes were targeted. Systemic GEM 150 mg/m^2 was administered weekly. Within 4–6 weeks after the completion of NACRT, the patients were reassessed by CT, MRI and PET-CT and surgery was performed. During the same period, 11 patients did not receive preoperative chemoradiotherapy but underwent surgery (the non-NACRT group).

Recurrence was diagnosed on the basis of clinical examinations and imaging studies. Time to death, final follow-up examination, and the diagnosis of recurrence was measured from the date of surgery. Surviving patients were followed up until March 2014.

Written informed consent was obtained from all 28 patients prior to their enrollment in the study, and this study design and protocol were approved by the institutional review board of Hokkaido University Hospital Sapporo, Japan (Clinical Research approval number 013–0074).

Pathological specimens

Formalin-fixed and paraffin-embedded specimens were retrieved from the surgical pathology files of the Pathology Department of Hokkaido University Hospital. Sections were cut and stained with hematoxylin-eosin (H&E) for routine histopathologic examination. Pancreatic ductal adenocarcinoma was diagnosed in all specimens. A representative tissue block was selected from each case to perform immunohistochemical studies.

Immunohistochemistry

The resected tissues were fixed in 10% formalin and embedded in paraffin blocks, and the most representative block was chosen for each case. Each block was cut into serial 4-μm-thick sections for staining with H&E and immunohistochemistry for EpCAM, CD24, CD44, CD133, CXCR4 and ALDH1. Immunohistochemistry was performed using the EnVision + System-HRP (Dako Japan, Tokyo), and the protocol was optimized for each antigen (Table 1).

Briefly, the sections were mounted on charged glass slides, deparaffinized, and rehydrated through a graded ethanol series. Antigens were retrieved in Dako EnVision FLEX Target Retrieval Solution using Dako PT Link for 20 min at 97°C according to the manufacturer's instructions (Dako Japan). After the blocking of endogenous peroxidase activity with 0.03% hydrogen peroxide, the sections were incubated with the primary antibodies at room temperature for 30 min and then reacted with a dextran polymer reagent combined with secondary antibodies and peroxidase for 30 min at room temperature. Specific antigen-antibody reactions were visualized with diaminobenzidine chromogen applied for 10 min. Slides were counterstained with hematoxylin, dehydrated and mounted.

Non-neoplastic pancreatic tissues on the same slides as those summarized in Table 1 were defined as internal positive controls for each antibody [17,19,27-29]. Negative control tissue sections were prepared by omitting the primary antibody.

Immunohistochemical evaluation

All assessments were made on the tumour region of the specimen (×200). Each slide was evaluated independently

Table 1 Primary antibodies used in the immunohistochemistry

Antigen (clone)	Location	Antibody species	Manufacturer (product)	Antigen-retrieval solution	Dilution	Internal positive control [reference No]
EpCAM (ESA)	M	Mouse monoclonal	Dako (M3525)	PH6 ciltrate buffer	1:200	Epithelium of pancreatic ducts, acinar cells and islets of Langerhans cells [29]
CD24	M	Mouse monoclonal	Neomarkers (MS-1279)	PH6 ciltrate buffer	1:50	Acinar cells [27]
CD44	M	Mouse monoclonal	Abcam(ab51037)	PH6 ciltrate buffer	1:50	Acinar cells [28]
CD133	M	Rabbit polyclonal	Abnova(12663)	PH9 Tris EDTA buffer	1:50	Acinar cells [19]
CXCR4	M	Mouse monoclonal	Zymed(35-8800)	PH6 ciltrate buffer	1:50	Acinar cells [17]
ALDH1	C	Mouse monoclonal	Abcam(ab52492)	PH6 ciltrate buffer	1:100	Acinar cells and islets of Langerhans cells [19]

M: membrane C: cytoplasm.

by two independent observers (authors TM and TM), who did not know the clinical outcomes, and discrepancies between the observers were resolved using a conference microscope. To take into account intratumoral heterogeneity of antigen expression, we selected two to six visual fields from different areas of invasive ductal carcinoma excluding that of intraepithelial neoplasia in each slide. In detail, guided by the microscope, the areas were selected randomly per section using a × 4 objective and a × 10 ocular lens on each H-E staining slide and marked it by circling each area. And then, we superimposed the slide which was stained with CSCs markers on the HE staining slide, and have marked it by tracing the mark for evaluation of the immunoreacting score (IRS). The immunoreaction for each antibody was evaluated in each case based on both the proportion of positive-stained tumour cells and the staining intensity of the tumour cells . The expression site of each antibody (membrane or cytoplasm) is given in Table 1. The expression of each antibody was evaluated for each tissue sample by calculating the total IRS as the product of the proportion and intensity scores according to previous reported criteria [22]. Briefly, the proportion score reflected the estimated fraction of positive-stained tumour cells (0, none; 1, 1%–10%; 2, 11%–50%; 3, 51%–80%; 4, 81%–100%). The intensity score represented the estimated staining intensity (0, no staining; 1, weak; 2, moderate; 3, strong). The total IRS ranged from 0 to 12, and the scores were averaged. A positive expression of each antibody was defined as an averaged score > median.

Statistical analysis

We used a t-test or Fisher's exact test to evaluate the differences in clinicopathological and immunohistological features between the NACRT and non-NACRT group. We tested the associations between clinicopathological and immunohistologically detected stem cell marker expressions by Fisher's exact test. Survival curves of patients were drawn by the Kaplan- Meier method. Differences in survival curves were analyzed by the log-rank test. Differences at $P < 0.05$ were considered significant. All statistical analyses were performed using JMP Pro 10 (SAS Institute Japan).

Results

Patient characteristics

The patient demographics are shown in Table 2. T-factor, N-factor, Histological classification and R-factor were assigned according to the TNM classification of the Union Internationale Contre le Cancer (UICC 7th edition). There were no significant differences between the NACRT and non-NACRT groups in age, gender, operative procedures, portal vein resection, clinical T, N factor, pathological T, N factor, histological classification, or residual tumour.

In the evaluation of tumour destruction, over 50% of the cancer cells had degenerated in nine patients.

Table 2 Patient demographics and clinicpathological characteristics

	NACRT (n = 17)	Non-NACRT (n = 11)	P-value
Age(mean ± SD)	59.9 ± 7.9	63.6 ± 10.4	0.287*1
Gender(male/female)	8/9	6/5	1.000*2
Operative procedures PD/DP/TP	13/3/1	10/1/0	1.000*2
Portal vein resection	70.6% (12/17)	63.6% (7/11)	1.000*2
cT(1/2/3/4)	0/0/17/0	0/0/11/0	1.000*2
cN(0/1)	11/6	6/5	0.701*2
pT(0/1/2/3/4)	0/1/16/0	0/0/11/0	1.000*2
pN(0/1)	13/4	5/6	0.125*2
Histological classification G1-2/G3/ungradeable	11/5/1	8/3/0	1.000*2
Residual tumor R0/R1-2	17/0	9/2	0.146*2
Tumor destruction (Evan's criteria)I/IIa/IIb/III/IV	1/7/7/2/0		

SD: standard deviation; PD: pancreatoducdenectomy; DP: distal pancreatectomy; TP total pancreatectomy. *1: Unpaired t-test. *2: Fisher's exact test.

Patterns of expression

The expressions of EpCAM, CD24, CD44, CD133, and CXCR4 antigens were membranous in carcinoma cells (Figure 1A–E).

The IRS of cancer cells with membranous EpCAM expression ranged from 0 to 12 (median 7.3). Using the cut-off point, of the 28 cases, 15 (53.6%) were considered positive. The IRS of the cancer cells with membranous CD44 expression ranged from 0 to 12 (median 3.4), with 16/28 (57.1%) cases considered positive. The IRS of the cancer cells with membrane CD24 expression ranged from 0 to 12 (median 2.9), with 10/28 (35.7%) cases being positive. The IRS of the cancer cells with membrane CD133 expression ranged from 1 to 12 with a median value of 5.7, and 15/28 (53.6%) cases were considered positive for CD133. The IRS of the cancer cells with membranous CXCR4 expression ranged from 1 to 12 (median 6.1), with 11/28 (39.3%) cases considered positive.

The expression of ALDH1 was cytoplasmic in carcinoma cells (Figure 1F). The IRS of the cancer cells with cytoplasmic ALDH1 expression ranged from 1 to 12 with a median value of 5.6. Of the 28 cases, 13 (46.4%) were considered positive.

Response analysis

As shown in Table 3, a positive CD44 expression was found in 14 of the 17 cases (82.4%) in the NACRT group and in 2 of the 11 cases (18.2%) in the non-NACRT group; the difference between the two groups was significant (P = 0.00148).

Positive CD133 expression was found in 5 of the 17 cases (29.4%) in the NACRT group and in 9 of the 11

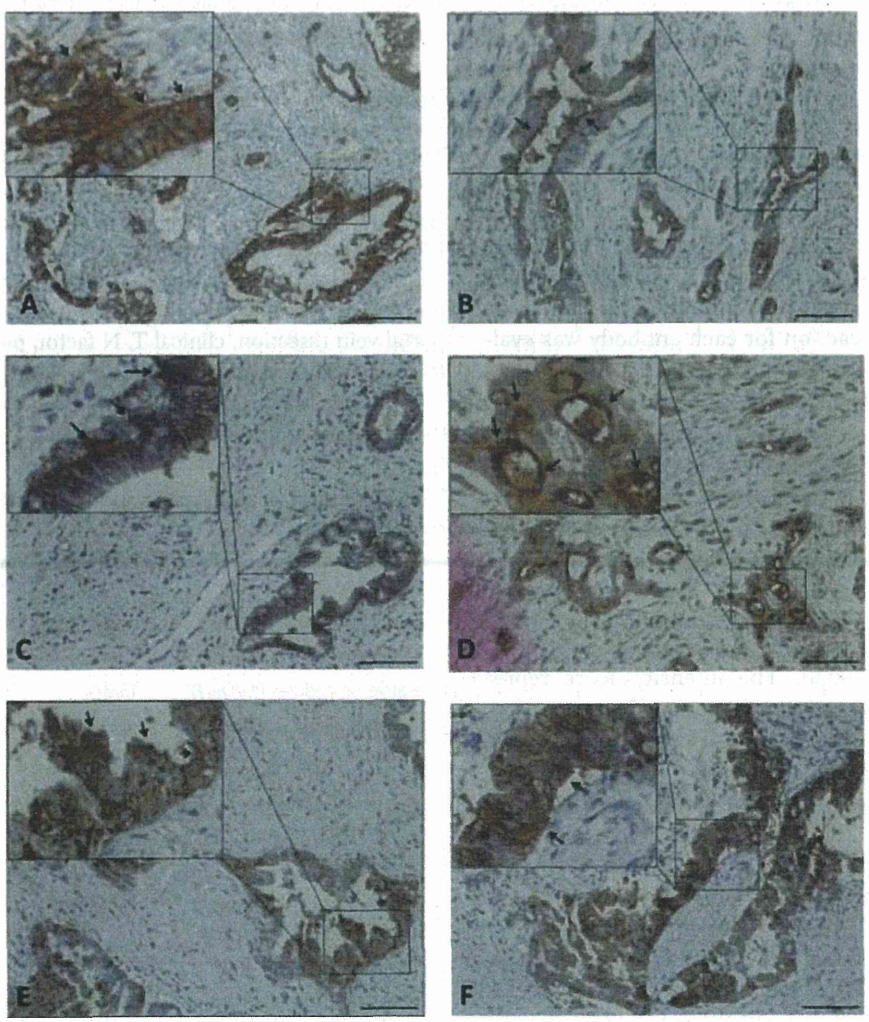

Figure 1 Immunohistochemical staining of each CSC marker in pancreatic adenocarcinoma. The arrows indicate strong staining intensity of EpCAM **(A)**, CD24 **(B)**, CD44 **(C)**, CD133 **(D)**, CXCR4 **(E)** and ALDH1 **(F)**. Scale bar, 100 μm.

Table 3 Frequency of CSCs markers positive cases

	NACRT(n = 17)	Non-NACRT(n = 11)	P-value
EpCAM(+)	58.8%	45.5%	0.700
CD24(+)	35.3%	36.4%	1.000
CD44(+)	82.4%	18.2%	**0.00148**
CD133(+)	29.4%	81.8%	**0.0183**
CXCR4(+)	47.1%	27.2%	0.435
ALDH1(+)	64.7%	18.2%	**0.0237**

Fisher's exact test.
The bold value indicates a statistically significant result.

cases (81.8%) in the non-NACRT group; the difference between the two groups was significant (P = 0.0183).

Positive ALDH1 expression was found in 11 of the 17 cases (64.7%) in the NACRT group and in 2 of the 11 cases (18.2%) in the non-NACRT group; the difference between the two groups was significant (P = 0.0237).

No significant differences were found in the frequency of expression of EpCAM, CD24 or CXCR4 between the NACRT group and the non-NACRT group.

Correlation among CSC markers

As shown in Table 4, CD133 expression was inversely related to ALDH1 expression in the NACRT group (P = 0.0276), but no significant associations were observed between the other CSCs markers.

Association with histopathological variables

Table 5 shows the associations of CSC markers with clinicopathologic features in the NACRT group. The positive expression of CXCR4 was significantly correlated with a higher liver metastasis rate (P = 0.0152).

Positive CD133 and negative ALDH1 expression had a markedly poorer OS

Figure 2 shows that the patients who underwent NACRT had significantly better disease-free survival (DFS) and overall survival (OS) rates compared to the patients who did not undergo NACRT (P = 0.0056 and P = 0.0158, respectively).

In the NACRT group, the patients with positive CD133 expression had a significantly poorer OS rate (P = 0.0406) compared to those with negative CD133 expression (Figure 3A).

However, the patients with positive expression of CD44 and ALDH1 had no significant differences in prognosis compared to the patients with negative expression of CD44 and ALDH1. In addition, the patients with positive CD133 and negative ALDH1 expression had a markedly poorer OS rate (P = 0.0039) compared to the patients with expressions of other markers (Figure 3B).

Discussion

In this study, we focused on EpCAM, CD24, CD44, CD133, CXCR4 and ALDH1 as representative pancreatic CSC markers and examined the effect of NACRT on pancreatic CSCs. Our major findings are as follows: (1) CD44- and ALDH1-positive cells may have chemoradiation resistance, but CD133-positive cells may have chemoradiation susceptibility in pancreatic cancer; (2) CD133 and ALDH1 expressions may be useful predictors of prognosis in pancreatic adenocarcinoma patients who have received NACRT. As the evaluation method of

Table 4 Correlations between CSC marker expressions in the NACRT group

	ESA			CD24			CD44			CD133			CXCR4		
	(+)	(-)	P	(+)	(-)	P	(+)	(-)	P	(+)	(-)	P	(+)	(-)	P
CD24															
(+)	4	2	1.000												
(-)	6	5													
CD44															
(+)	9	5	0.537	4	10	0.515									
(-)	1	2		2	1										
CD133															
(+)	3	2	1.000	3	2.280	5	0	0.515							
(-)	7	5		3	9	9	3								
CXCR4															
(+)	4	4	0.637	4	4	0.335	6	2	0.576	2	6	1.000			
(-)	6	3		2	7		8	1		3	6				
ALDH1															
(+)	7	4	0.644	3	8	0.600	9	2	1.000	1	10	**0.0276**	5	6	1.000
(-)	3	3		3	3		5	1		4	2		3	3	

Fisher's exact test.
The bold value indicates a statistically significant result.

Table 5 Association of CSC markers with clincopathologic features in the NACRT group

Parameter	Total	EpCAM (+) (n = 10)	p	CD24 (+) (n = 6)	p	CD44 (+) (n = 14)	p	CD133 (+) (n = 5)	p	CXCR4 (+) (n = 8)	p	ALDH1 (+) (n = 11)	p
Histological classification													
Grade 1/2	11	8	0.186	4	0.547	9	1.000	4	0.0801	3	0.0633	8	0.547
Grade 3	5	2		1		4		0		4		3	
ungradeable	1	0		1		1		1		1		0	
ypT													
ypT2	1	1	1.000	0	1.000	1	1.000	0	1.000	0	1.000	1	1.000
ypT3	16	9		6	13			5		8		10	
ypN													
ypN1	4	3	0.603	2	0.584	3	1.000	2	0.538	2	1.000	3	1.000
ypN0	13	7		4		11		3		6		8	
Tumour down stage													
Present	5	4	0.338	2	1.000	5	0.515	1	1.000	4	0.131	3	1.000
Absent	12	6		4		9		4		4		8	
Lymphatic invasion													
Present	1	0	1.000	0	1.000	1	1.000	0	1.000	0	1.000	1	1.000
Absent	16	10		6		13		5		8		10	
Blood vessel invasion													
Present	11	7	0.644	3	0.600	9	1.000	3	1.000	4	0.335	7	1.000
Absent	6	3		3		5		2		4		4	
Perineural invasion													
Present	12	6	0.338	3	0.280	10	1.000	3	0.600	6	1.000	8	1.000
Absent	5	4		3		4		2		2		3	
Recurrence													
Present	11	6	1.000	5	0.333	10	0.515	4	0.600	7	0.131	7	1.000
Absent	6	4		1		4		1		1		4	
Liver metastasis													
Present	7	3	0.350	3	0.644	6	1.000	2	1.000	6	**0.0152**	6	0.304
Absent	10	7		3		8		3		2		5	
Tumor destruction (Evans's criteria)													
I/IIa	8	5	1.000	1	0.131	7	1.000	1	0.294	3	0.637	5	1.000
IIb/III	9	5		5		7		4		5		6	

Fisher's exact test.
The bold value indicates a statistically significant result.

the effect of NACRT, we compared the expression of several CSC markers immunohistochemically detected in human pancreatic cancer specimens from patients who received and did not receive NACRT. Although the comparison of tissue samples obtained from the same individual before and after NACRT is desirable, the evaluation has been difficult in terms of the quantity and quality of biopsy material before NACRT. Thus, we think that comparisons between patients in similar cohorts who received and did not receive NACRT are adequate to determine whether the survival of CSC marker-positive cells is a phenomenon that occurs in human cancer tissue.

Regarding the chemoradiation resistance to pancreatic CSCs, we have demonstrated that the frequencies of CD44- and ALDH1-positive cases are increased in the NACRT group. This result indicates that CD44- and ALDH1-positive cells may have chemoradiation resistance in pancreatic cancer. CD44 is involved in cell-to-cell and cell-to-matrix interactions and has been used